Highly controllable transparent and conducting thin films using layer-by-layer assembly of oppositely charged reduced graphene oxides†‡

Dong Wook Lee, Tae-Keun Hong, Dongwoo Kang, Jisook Lee, Mihee Heo, Jin Young Kim, Byeong-Su Kim* and Hyeon Suk Shin*

A new approach for the fabrication of reduced graphene oxide (rGO) multilayers which can be used for transparent and conducting thin films was developed. This was achieved by using layer-by-layer (LbL) assembly of positively and negatively charged rGO sheets, which could provide highly controllable thin films in terms of thickness, transmittance, and sheet resistance. In particular, the thickness of the multilayer thin films of rGO was able to be controlled precisely in the subnanometre scale by ~0.46 nm via simply varying the number of stacking layers. Therefore, this method enabled an excellent control of the rGO multilayers over the optical and electrical properties, which are related to the thickness. Furthermore, we demonstrated the application of the rGO multilayers for an OLED device.

Introduction

Graphene, a single layer of two-dimensional carbon lattice, has recently emerged as a promising novel nanomaterial with its remarkable electrical, chemical and mechanical properties.[1–3] Graphene has the potential to affect the development of new generations in quantum devices, nanocomposites, and ultrathin membranes. While earlier fundamental researches have been initiated from the micromechanical cleavage of highly crystalline graphite for high-quality graphene sheets,[1–3] recent efforts are geared toward producing the graphene sheets in a controlled, scalable, and reproducible manner. For example, stable suspensions of reduced graphene oxide (rGO) can be readily obtained by ultrasonication of chemically oxidized graphite oxide, offering the potential of creating large-scale graphene thin films.[4] A number of approaches have been made to assemble these well-dispersed oxidized or chemically reduced graphene oxide nanosheets into thin films with tailorable properties. They include vacuum filtration,[5–10] dip coating,[11,12] spin-coating,[13–16] Langmuir–Blodgett assembly,[17,18] and direct chemical vapor deposition.[19,20]

The LbL assembly has been so far used to make thin films consisting of poly(acrylic acid)-modified and poly(acryl amide)-modified graphene nanoplatelets or negative-charged graphite oxide and positive-charged polymer like poly(allylamine hydrochloride).[21,22] These LbL assemblies were limited to the hybrid structures with organic materials like charged polymers that can degrade intrinsic electrochemical or electronic property of graphene. Alternatively, herein, we present a simple and facile approach of exclusively integrating the graphene sheets into the multilayers by layer-by-layer (LbL) assembly process, which can create highly controllable, conformal thin films in terms of thickness, transmittance, and sheet resistance. We have constructed LbL multilayers with a sheet resistance of 2.5 KΩ sq^{-1} at a transmittance of 75% by employing the electrostatic interactions between oppositely charged exfoliated nanosheets of rGO (Scheme 1). The advantage of this approach is that the thickness of the multilayer thin films of rGO is able to be controlled precisely in the subnanometre scale by ~0.46 nm via simply varying the number of stacking layers. This method affords ultrathin multilayers of rGO with an excellent control over the optical and electrical properties as well because these properties are correlated with the thickness. Very recently, we showed that this approach could successfully expand to integrate only active carbon nanomaterials such as rGO and multi-walled carbon nanotubes at a nanoscale precision for fine tuning the electrical and optical properties.[23] In this study, furthermore, we demonstrate the application of the assembled graphene thin film as a transparent, conducting electrode for an organic light-emitting diode.

Interdisciplinary School of Green Energy, UNIST (Ulsan National Institute of Science and Technology), Banyeon-ri 100, Ulsan, 689-798, Republic of Korea. E-mail: shin@unist.ac.kr; bskim19@unist.ac.kr
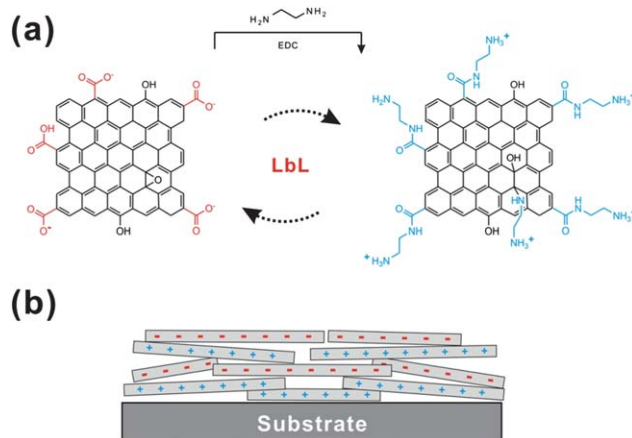
Scheme 1 Schematic representation of LbL assembly of reduced graphene oxide multilayer with rGO–COO⁻ and rGO–NH₃⁺ (a) and the resulting LbL film of rGO (b).

Experimental

Preparation of negatively and positively charged GO and rGO

Graphite oxide was synthesized by modified Hummers method,[7,24] and exfoliated to give a brown dispersion of graphene oxide under ultrasonication. The resulting graphene oxide (GO) is negatively charged over a wide pH condition since the GO sheet has chemical functional groups such as carboxylic acids. Positively charged GO was synthesized by using N-ethyl-N'-(3-dimethyl aminopropyl)carbodiimide methiodide (EDC, 98%, Alfa Aesar) and ethylenediamine (99%, Sigma-Aldrich).[23,25,26] Negatively charged GO suspension (50 mL) was combined with EDC (600 mg) and ethylenediamine (4 mL) and stirred for 4 h, and afterwards the mixture solution was dialyzed for 24 h to remove EDC and ethylenediamine. The MWCO of the dialysis tubing (Spectra/Por dialysis membrane) is 12–14 kD. Then positively charged GO suspension of dark brown color was obtained. Negatively and positively charged GO suspensions were reduced by hydrazine solution (35 wt% in water, Aldrich). As-prepared negatively charged GO suspension (5.0 mL) was mixed with 5.0 μL of hydrazine solution and 35.0 μL of ammonia solution (28–30%, Samchun) in a 20 mL glass vial. After stirring for a few minutes, the vial was put in a water bath at 95 °C for 1 h. The reduction of positively charged GO suspension was identically carried out without mixing of the ammonia solution.

Layer-by-layer assembly

Silicon or quartz substrate was cleaned by piranha solution to remove any organic contamination and treated with oxygen plasma to introduce hydrophilic surface. Positively charged rGO (or GO) solution (0.5 mg mL^{-1}) at pH 10 was dropped on the silicon or quartz substrate which was loaded in a spin coater (ACE-200, Dong Ah Tech), maintained for 2 min as a waiting period, and spun at 3000 rpm for 30 seconds. As a rinsing step, DI water at the same pH was dropped on the substrate coated with positively charged rGO, maintained for 2 min, and spun at 3000 rpm for 30 seconds. Next, negatively charged rGO (or GO) solution (0.5 mg mL^{-1}) at pH 10 was spin-coated with the same procedures, followed by the rinsing step. Then, we obtained one bilayer of rGO sheets. The above procedures were repeated to achieve the desired number of bilayers.

Fabrication of OLED device

ITO-coated glass (10 Ω sq^{-1}) and rGO-coated glass (3 kΩ sq^{-1}) substrates were used for making polymer light-emitting devices, respectively. The electroluminescence properties depending on each electrode were studied in the structure of ITO/poly(3,4-ethylenedioxythiophene):poly(styrenesulfonate) (PEDOT:PSS)/poly(2-methoxy-5-(2′-ethylhexyloxy)-1,4-phenylene vinylene) (MEH-PPV)/Ba/Al and rGO/PEDOT:PSS/MEH-PPV/Ba/Al, respectively. The current density (J), luminance (L), and luminous efficiency of each device were measured using a Keithley 2365A source measure unit equipped with Minolta CS2000. Measurements were performed under air ambient room temperature condition, but samples were stored in a N$_2$-filled glove box to avoid photo-oxidation. The total time of exposure to air was kept less than 10 minutes.

Characterization methods

Amine-functionalized GO sheets were characterized by XPS (Thermo Fisher, K-alpha). AFM images were measured in tapping mode with Nanoscope V from Veeco. The thickness of rGO and GO multilayers on the silicon substrate was measured by ellipsometry (J. A. Woollam Co. Inc, EC-400 and M-2000V). The average thickness values after three measurements were provided. The transmittance of the graphene films was characterized by using the UV/VIS spectroscopy (VARIAN, Cary 5000). Raman spectra were obtained with Alpha 300s from WITEC. The resistance of the graphene films was measured by using the four-point probe method (AIT, CMT-SR1000N).

Results and discussion

To introduce the rGO into an LbL system based on the electrostatic interactions, initially graphene oxide suspensions were prepared according to the modified Hummers method.[24] Following the sonication for exfoliation of graphite oxide, the chemical functional groups introduced on the surface of graphene sheet such as carboxylic acids (COOH) render the prepared GO negatively charged over a wide pH condition (GO–COO$^-$) (see ζ-potential measurements in Fig. S1 of ESI†). Subsequently, positively charged GO sheets were prepared by introducing amine groups (NH$_2$) on the surface of negatively charged GO sheets through the N-ethyl-N'-(3-dimethyl aminopropyl)carbodiimide methiodide (EDC) mediated reaction between carboxylic acids (and/or epoxides) and excess ethylenediamine, which leads to positively charged stable GO suspension (GO–NH$_3^+$). Chemical reduction of each GO suspension was carried out by adding hydrazine in the presence of ammonia to prevent the aggregation of the resulting rGO suspensions as reported previously.[7] As demonstrated in ζ-potential measurements, the prepared rGO suspensions exhibit a fairly good colloidal stability over a wide span of pH conditions (see Fig. S1, ESI†). X-Ray photoelectron spectroscopy (XPS) further supports the presence of the surface functional groups after the introduction of amine groups (see Fig. S2 in ESI†).

Based on the electrostatic interactions, multilayer thin films were assembled by repeatedly layering the suspensions of rGO–NH$_3^+$ and rGO–COO$^-$ on a planar silicon wafer or quartz slide to afford the multilayer in the architecture of (rGO–NH$_3^+$/rGO–COO$^-$)$_n$ (n = number of bilayer) (Scheme 1). We chose pH 10 for spin-assisted LbL assembly of both rGO–NH$_3^+$ and rGO–COO$^-$ with an optimum colloidal stability and sufficient surface charges. The spin-coating method was used in the LbL assembly because it had several advantages over dip coating and spray coating methods in terms of transmittance, thickness control, and time of film fabrication. The fabrication of the multilayers was monitored by the gradual increase of characteristic UV/Vis absorbance of rGO at 268 nm (λ_{max}) (Fig. 1(a)). In comparison to the absorption peak of GO suspension at 227 nm, the shifted absorption maxima of rGO multilayer film indicate that the electronic conjugation within the graphene sheets was restored upon chemical reduction. In consistency with the absorption spectra, the ellipsometric measurement provides that the thickness of rGO multilayer films was linearly proportional to the number of bilayers (Fig. 1(b)). The as-prepared rGO multilayer
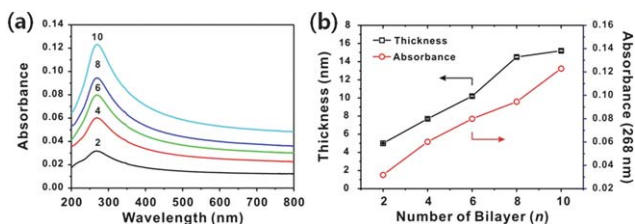
Fig. 1 Growth curve of (rGO–NH$_3$$^+$/rGO–COO$^-$)$_n$ multilayer. (a) UV/Vis spectra of the multilayer deposited on a quartz slide and (b) a plot of thickness and absorbance with respect to the number of bilayer. The film thickness was measured by ellipsometry.

films could not be used directly for transparent electrodes due to their high sheet resistance. Therefore, an annealing process at 1000 °C in H$_2$ atmosphere, which is similar to the methods reported elsewhere,[4,15,16] was introduced and then the sheet resistance decreased by two orders relative to the as-prepared multilayers (see Fig. S3 in ESI†).

The surface morphology of rGO multilayers was observed by atomic force microscopy (AFM) before and after annealing. We can observe the edges of individual sheets of graphene clearly in as-prepared samples before annealing (Fig. 2(a–d)). In particular, the initial film with 2 bilayers in Fig. 2(b) shows obviously individual, separated sheets of rGO, whereas the film with 10 bilayers in Fig. 2(d) shows overlaid sheets which make it difficult to identify edges (see Fig. S4† for the AFM height profiles). Surface root-mean-square (rms) roughness (R_q) is determined to be 0.94 and 3.08 nm for 2 bilayers with 5.0 ± 0.06 nm thickness and 10 bilayers with 15.2 ± 0.12 nm thickness, respectively, from AFM images over 10 × 10 μm regions of Fig. 2(a) and (c). It is not strange that the surface rms roughness increases with the number of bilayers. The surface morphology of the multilayers is changed after annealing in the H$_2$ atmosphere at 1000 °C which was performed in order to improve the conductivity of the resulting graphene thin films. Fig. 2(e–h) show that individual sheets seem to merge together and so it is difficult to find the

distinct boundary of each sheet in overlaid sheets. Such phenomenon is obviously observed in Fig. 2(h) with 10 bilayers that do not have vacant sites as shown in Fig. 2(f) with 2 bilayers. In Fig. 2(h), the individual sheets are not resolved, instead some wrinkles are observed in the uniform film. Such morphologies of 2 and 10 bilayers after annealing were identically observed in SEM images (see Fig. S5 in ESI†). It is also of note that the surface rms roughness in AFM images over 10 × 10 μm regions after annealing reduced to 0.69 and 0.96 nm for 2 bilayers with 5.2 ± 0.02 nm thickness and 10 bilayers with 12.0 ± 0.31 nm thickness, respectively, in Fig. 2(e) and (g). Changes in the surface morphology and rms roughness may be due to the reorientation of rGO sheets and densification of the thin film during annealing. The above results on the changes of the surface morphology and the roughness in the rGO multilayers after annealing are similarly observed in GO multilayers. (GO multilayers were fabricated to compare with rGO multilayers. This will be discussed later. See Fig. S6 in ESI† for AFM images of GO multilayers.)

Fig. 3 exhibits the resulting sheet resistance and transmittance of rGO multilayers as a function of the number of bilayers after annealing. The sheet resistance decreases linearly with increasing number of bilayers in the region above 4 bilayers. Too high sheet resistance in the 2 bilayer is considered to be due to the imperfect connection of rGO sheets. The transmittance measured at 550 nm decreases gradually with increasing number of bilayers. In the present study, the lowest sheet resistance is 2.5 kΩ sq^{-1} at 75% transmittance. Even though the conductivity is not a superior result, it is comparable to the results reported previously.[4,13–15] If we consider the LbL assembly as proven in Fig. 2 and 3, the sheet resistance and transmittance can be easily changed in conjunction with the number of bilayers which is strongly related to the thickness of the multilayers. It means that we can precisely control the thickness, sheet resistance, and transmittance of the multilayers by fully taking advantages of nanoscale engineering of the LbL assembly.

To prove the precise control of the thickness, we show relationship between the number of bilayers and the thickness by
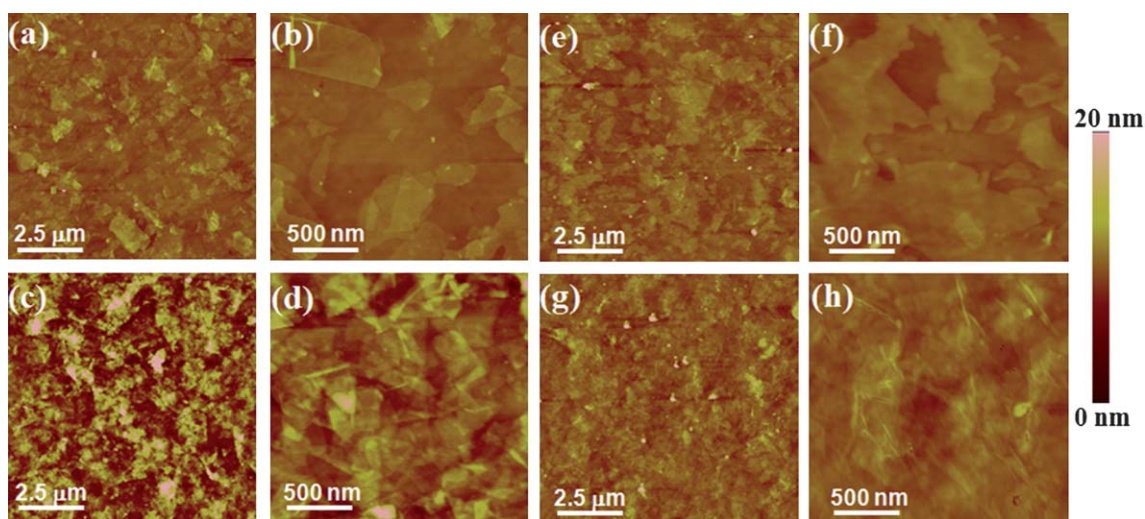
Fig. 2 AFM images of rGO multilayers on quartz substrates before (a–d) and after (e–h) annealing in H$_2$ atmosphere at 1000 °C for $n = 2$ bilayers (top panels: a, b, e, and f) and 10 bilayers (bottom panels: c, d, g, and h). Scale bar is 2.5 μm and 500 nm as indicated, respectively.
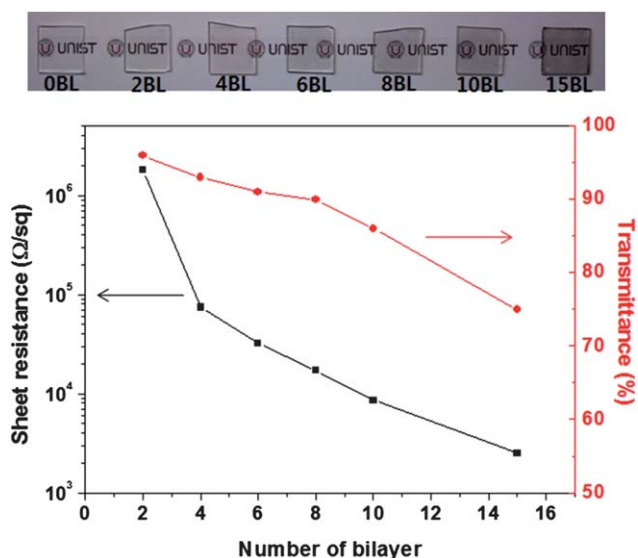
Fig. 3 Sheet resistance and transmittance of rGO multilayers after annealing in H_2 atmosphere at 1000 °C. Transmittance was measured at 550 nm. The top image shows a photograph for 0, 2, 4, 6, 8, 10, and 15 bilayers (BL) of rGO multilayers deposited on a quartz substrate after annealing.
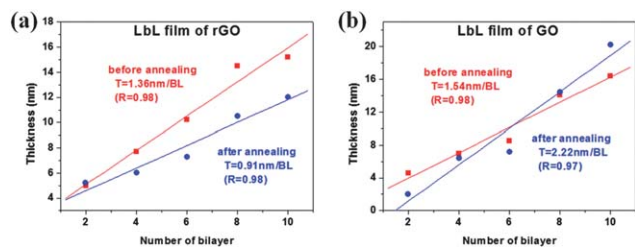
Fig. 4 Thickness of LbL multilayer thin films of rGO (a) and GO (b) before and after annealing.

ellipsometry. In the plot of the thickness vs. the number of bilayers in Fig. 4, red and blue curves correspond to the linear fits of the thickness data before and after annealing, respectively. The linear fit is determined to be valid from the value of $R = 0.98$. Thus, the slope of the fitted curve means the thickness per bilayer (nm per bilayer). In the fitted curves of rGO LbL films in Fig. 4(a), the slopes are 1.36 and 0.91 nm per bilayer before and after annealing, respectively. The decrease in the thickness per bilayer after annealing is due to the removal of functional groups remaining even in the rGO sheets. The above results indicate that the thickness of the multilayer is linearly proportional to the number of layers by LbL assembly and the thickness of one layer in rGO multilayers after annealing is 0.46 nm. Thus, we could reach the conclusion that the thickness of the multilayer thin film of rGO is able to be controlled precisely in the subnanometre scale by ~0.46 nm via simply varying the number of stacking layers. This method affords ultrathin multilayers of rGO with an excellent control over the optical and electrical properties because the properties are correlated with the thickness.

To compare with rGO multilayers, GO sheets can be used as starting materials for the fabrication of transparent and conducting electrode as reported in the other papers.[4,15,16] All fabrication procedures for GO multilayers that do not include any chemical reduction step are the same as those for rGO multilayers. Characterization results such as UV/Vis absorption and AFM supported a successful fabrication of GO multilayers by LbL assembly (see Fig. S6 in ESI†). We compare the thickness per bilayer in GO multilayers with that in rGO multilayers. From the slopes of the fitted curves in Fig. 4(b), the thickness is 1.54 and 2.22 nm per bilayer before and after annealing. On the contrary to rGO multilayers, the thickness of GO multilayers increases after annealing. This may be due to more gases generated during annealing which are originated from much more oxygenated functional groups in GO sheets than in rGO sheets, eventually expanding the multilayer sheets. Different internal structures between rGO and GO sheets are expected to induce different properties. Actually, values of sheet resistance at the same transmittance are different between the rGO and GO sheets. Multilayers of rGO show 8.6 and 32 kΩ sq^{-1} at 86 and 91% transmittance, whereas GO multilayers show 21 and 67 kΩ sq^{-1} at 88 and 91% transmittance. Another difference between the rGO and GO sheets is the extent of reduction in transmittance after annealing with increasing number of bilayers. The rGO multilayers showed reduction by only 1–2% in transmittance after annealing, whereas the GO multilayers showed reduction by 9% at 10 bilayers in transmittance after annealing
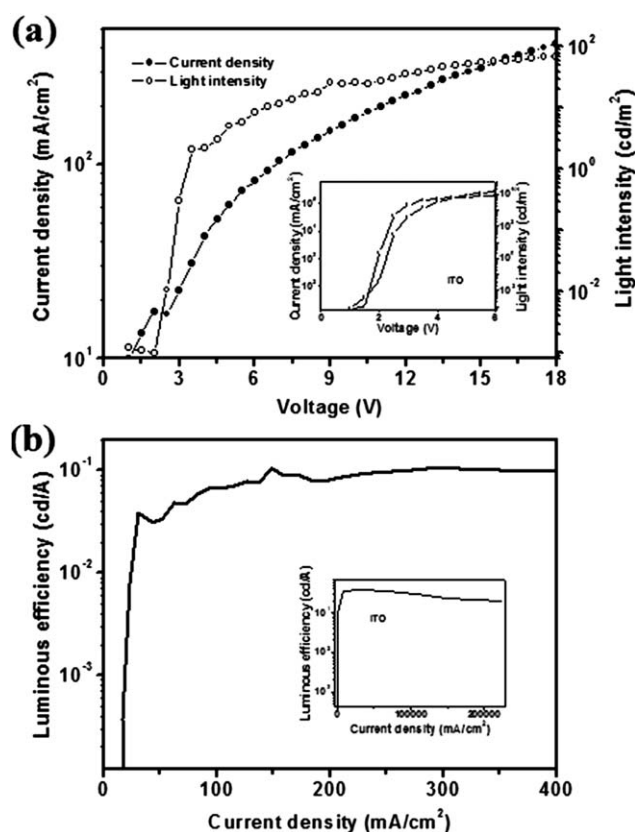
Fig. 5 (a) Current density–voltage–luminance (J–V–L) characteristic of the OLED device using the rGO electrode with 3 kΩ sq^{-1}. The inset is the electroluminescence property of the device fabricated with the ITO electrode. (b) Luminous efficiency of the device with the rGO electrode. The inset is luminous efficiency of the device fabricated with the ITO electrode.

(see Fig. S3 and S6 in ESI†). In comparison of Raman spectra before and after annealing, both multilayers showed a similar trend that the ratio of I_D/I_G decreased from 2.60 to 2.15 for rGO multilayers and from 2.57 to 2.30 for GO multilayers (see Fig. S7 in ESI†).

Lastly, we show that the rGO multilayers by LbL assembly can be used as transparent electrodes for organic light-emitting diode (OLED) devices. The current density–voltage–luminance $(J–V–L)$ characteristics of the devices fabricated on the ITO and graphene-coated substrate, respectively, are shown in Fig. 5. In comparison with the ITO electrode device which shows the maximum luminance of $\sim$7800 cd m^{-2} at 6 V as seen in the inset of Fig. 5(a), the maximum luminance of the rGO electrode device is $\sim$70 cd m^{-2} at 18 V and increases with applied bias voltage in Fig. 5(a). Fig. 5(b) shows the luminous efficiency of the devices with ITO and rGO electrodes. The maximum luminous efficiency of the device with the rGO electrode is $\sim$0.10 cd A^{-1} as shown in Fig. 5(b), while that with the ITO electrode is $\sim$0.38 cd A^{-1} as shown in the inset of Fig. 5(b).

Conclusion

We have developed a novel method of integrating the rGO and GO sheets into the LbL multilayer thin films. This approach employs the electrostatic interactions of two oppositely charged suspensions of rGO and GO sheets. The prepared multilayers exhibited tunable thickness, sheet resistance, and transmittance with respect to the number of bilayers. Moreover, the rGO multilayer was used as a transparent electrode in an OLED device. Therefore, the successful LbL assembly in this study would enable various research and developments for real applications since it makes highly controllable rGO thin film in large scale and combination of graphene and other functional nanomaterials possible.

Acknowledgements

Reference

1 K. S. Novoselov, A. K. Geim, S. V. Morozov, D. Jiang, Y. Zhang, S. V. Dubonos, I. V. Grigorieva and A. A. Firsov, *Science*, 2004, **306**, 666.
2 K. S. Novoselov, D. Jiang, F. Schedin, T. J. Booth, V. V. Khotkevich, S. V. Morozov and A. K. Geim, *Proc. Natl. Acad. Sci. U. S. A.*, 2005, **102**, 10451.
3 A. K. Geim and K. S. Novoselov, *Nat. Mater.*, 2007, **6**, 183.
4 G. Eda, G. Fanchini and M. Chhowalla, *Nat. Nanotechnol.*, 2008, **3**, 270.
5 D. A. Dikin, S. Stankovich, E. J. Zimney, R. D. Piner, G. H. B. Dommett, G. Evmenenko, S. T. Nguyen and R. S. Ruoff, *Nature*, 2007, **448**, 457.
6 Y. Xu, H. Bai, G. Lu, C. Li and G. Shi, *J. Am. Chem. Soc.*, 2008, **130**, 5856.
7 D. Li, M. B. Muller, S. Gilje, R. B. Kaner and G. G. Wallace, *Nat. Nanotechnol.*, 2008, **3**, 101.
8 B.-S. Kong, H.-W. Yoo and H.-T. Jung, *Langmuir*, 2009, **25**, 11008.
9 S. Park, J. An, I. Jung, R. D. Piner, S. J. An, X. Li, A. Velamakanni and R. S. Ruoff, *Nano Lett.*, 2009, **9**, 1593.
10 B.-S. Kong, J. Geng and H.-T. Jung, *Chem. Commun.*, 2009, 2174.
11 X. Wang, L. Zhi and K. Mullen, *Nano Lett.*, 2008, **8**, 323.
12 Y. Zhu, W. Cai, R. D. Piner, A. Velamakanni and R. S. Ruoff, *Appl. Phys. Lett.*, 2009, **95**, 103104.
13 H. Yamaguchi, G. Eda, C. Mattevi, H. Kim and M. Chhowalla, *ACS Nano*, 2010, **4**, 524.
14 X. Wang, L. Zhi, N. Tsao, Ž. Tomović, J. Li and K. Müllen, *Angew. Chem., Int. Ed.*, 2008, **47**, 2990.
15 H. A. Becerril, J. Mao, Z. Liu, R. M. Stoltenberg, Z. Bao and Y. Chen, *ACS Nano*, 2008, **2**, 463.
16 L. Yanyu, et al., *Nanotechnology*, 2009, **20**, 434007.
17 X. Li, G. Zhang, X. Bai, X. Sun, X. Wang, E. Wang and H. Dai, *Nat. Nanotechnol.*, 2008, **3**, 538.
18 L. J. Cote, F. Kim and J. Huang, *J. Am. Chem. Soc.*, 2009, **131**, 1043.
19 K. S. Kim, Y. Zhao, H. Jang, S. Y. Lee, J. M. Kim, K. S. Kim, J.-H. Ahn, P. Kim, J.-Y. Choi and B. H. Hong, *Nature*, 2009, **457**, 706.
20 X. Li, Y. Zhu, W. Cai, M. Borysiak, B. Han, D. Chen, R. D. Piner, L. Colombo and R. S. Ruoff, *Nano Lett.*, 2009, **9**, 4359.
21 J. Shen, Y. Hu, C. Li, C. Qin, M. Shi and M. Ye, *Langmuir*, 2009, **25**, 6122.
22 N. I. Kovtyukhova, P. J. Ollivier, B. R. Martin, T. E. Mallouk, S. A. Chizhik, E. V. Buzaneva and A. D. Gorchinskiy, *Chem. Mater.*, 1999, **11**, 771.
23 T.-K. Hong, D. W. Lee, H. J. Choi, H. S. Shin and B.-S. Kim, *ACS Nano*, 2010, **4**, 3861.
24 W. S. Hummers and R. E. Offeman, *J. Am. Chem. Soc.*, 1958, **80**, 1339.
25 S. Bittolo Bon, L. Valentini and J. M. Kenny, *Chem. Phys. Lett.*, 2010, **494**, 264.
26 S. W. Lee, B.-S. Kim, S. Chen, Y. Shao-Horn and P. T. Hammond, *J. Am. Chem. Soc.*, 2009, **131**, 671.